

The Large-Scale Polarization of the Microwave Background and Foreground

Angélica de Oliveira-Costa¹, Max Tegmark¹, Chris O'Dell², Brian Keating³, Peter Timbie⁴,
George Efstathiou⁵ & George Smoot⁶

¹*Department of Physics & Astronomy, University of Pennsylvania, Philadelphia, PA 19104, USA,
angelica@higgs.hep.upenn.edu*

²*Department of Astronomy, University of Massachusetts, Amherst, MA 01003, USA*

³*Department of Physics, California Institute of Technology, Pasadena, CA 91125, USA*

⁴*Department of Physics, University of Wisconsin, Madison, WI 53706-1390, USA*

⁵*Institute of Astronomy, University of Cambridge, Cambridge CB3 0HA, UK*

⁶*Department of Physics, University of California, Berkeley, CA 94720, USA*

(December 2, 2024. To be submitted to Phys. Rev. D.)

The DASI discovery of CMB polarization has opened a new chapter in cosmology. Most of the useful information about inflationary gravitational waves and reionization is on large angular scales where Galactic foreground contamination is the worst, so a key challenge is to model, quantify and remove polarized foregrounds. We use the POLAR experiment, COBE/DMR and radio surveys to provide the strongest limits to date on the TE cross power spectrum of the CMB on large angular scales and to quantify the polarized synchrotron radiation, which is likely to be the most challenging polarized contaminant for the MAP satellite. We find that the synchrotron E - and B -contributions are equal to within 10% from 408 – 820MHz with a hint of E -domination at higher frequencies. We quantify Faraday Rotation and Depolarization effects in the two-dimensional (ℓ, ν) -plane and show that they cause the synchrotron polarization percentage to drop both towards lower frequencies and towards lower multipoles.

I. INTRODUCTION

The recent discovery of cosmic microwave background (CMB) polarization by the DASI experiment [1] has opened a new chapter in cosmology – see Figure 1. Although CMB polarization on degree scales and below can sharpen cosmological constraints and provide important cross-checks [2,3], the potential for the most dramatic improvements lies on the largest angular scales where it provides a unique probe of the reionization epoch and primordial gravitational waves. For instance, forecasts [4,5] indicate that the MAP satellite can measure the reionization optical depth τ seventeen times more accurately using polarization information, and that polarization increases the sensitivity of the Planck satellite to tensor modes by a factor of 25.

Unfortunately, these large scales are also the ones where polarized foreground contamination is likely to be most severe, both because of the red power spectra of diffuse Galactic synchrotron and dust emission and because they require using a large fraction of the sky, including less clean patches. The key challenge in the CMB polarization endeavor will therefore be modeling, quantifying and removing large-scale polarized Galactic foregrounds. This is the topic of the present paper. We will use the POLAR experiment to provide the strongest limits to date on cross-polarized microwave background and foreground fluctuations on large angular scales, and employ polarization sensitive radio surveys to further quantify the polarized synchrotron radiation, which is likely to be the most challenging contaminant in the polarization maps expected from the MAP satellite.

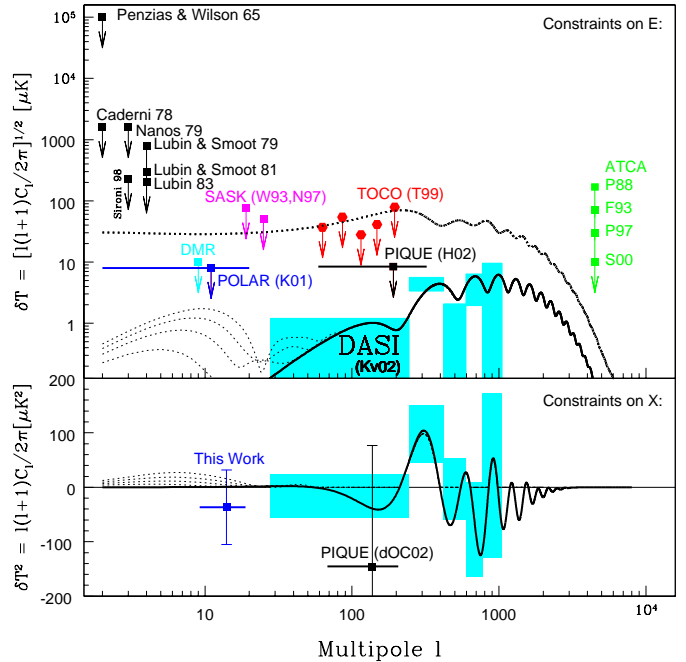


FIG. 1. Summary of constraints on polarization so far. From top to bottom, the three curves show the concordance model predictions for C_ℓ^T , C_ℓ^E and C_ℓ^X , respectively. Four reionization models with $\tau=0.1, 0.2, 0.3$ and 0.4 are also plotted (left thin lines from bottom to top in both plots). The limits for E are shown in the upper panel: Penzias & Wilson 65 [6], Caderni 78 [7], Nanos 79 [8], Lubin & Smoot 79 [9], Lubin & Smoot 81 [10], Sironi 98 [11], Lubin 83 [12], SASK (W93 [13], N97 [14]), TOCO (T99 *hexagons* [15]), P88 [16], F93 [17], P97 [18], S00 [19], DMR [20], PIQUE (H02 [21]) and POLAR (K01 [22]). The limits for X are shown in the lower panel: PIQUE (d0C02 [23]) and POLAR (“This Work”). The shaded regions are the DASI results (Kv02 [1]).

At microwave frequencies, three physical mechanisms are known to cause foreground contamination: synchrotron, free-free and dust emission. When coming from extragalactic objects, this radiation is usually referred to as point source contamination and affects mainly small angular scales. When coming from the Milky Way, this diffuse Galactic emission fluctuates mainly on the large angular scales that are the focus of this paper. Except for free-free emission, all the above mechanisms are known to emit polarized radiation. In the near term, the best measurement of large-scale polarization will probably come from the MAP satellite. At MAP's frequency range (22-90 GHz), synchrotron radiation is likely to be the dominant polarized foreground [4]. Unfortunately, we still know basically nothing about the polarized contribution of the Galactic synchrotron component at CMB frequencies [4,24–29], since it has only been measured at lower frequencies and extrapolation is complicated by Faraday Rotation. This is in stark contrast to the CMB itself, where the expected polarized power spectra and their dependence on cosmological parameters has been computed from first principles to high accuracy [30–33].

Polarization of the Galactic continuum emission was first clearly detected in 1962 [34]. In the succeeding years, polarization measurements of the northern sky were made at frequencies between 240 and 1415 MHz (see [35] and references therein) with resolutions of only a few degrees. No large-area survey has been published since the compendium of Brouw and Spoelstra [36] and high-resolution surveys have only begun to be made recently. The first major investigation done after [36] is that of [37], who observed a section of the Galactic plane defined by $49^\circ \leq \ell \leq 76^\circ$ and $|b| \leq 15^\circ$, at frequency of 2.7 GHz. The study of [38] provides the highest resolution insight into the small-scale structure of the Galaxy; however, this only covered a few areas of the sky which were not larger than a degree or so across. Recently, two fully-sampled polarimetric surveys were done at frequencies at 2.4 GHz [39,40] and at 1.4 GHz [41,42]. All of these high-resolution surveys covered only regions near the Galactic plane, so in order to use them for inferences relevant to CMB experiments, they need to be extrapolated both in Galactic latitude and in frequency.

The rest of this paper is organized as follows. In section Section II, we review the basics of CMB and synchrotron polarization as well as our methods for measuring and modeling it. We present our results in Section III and discuss our conclusions in Section IV.

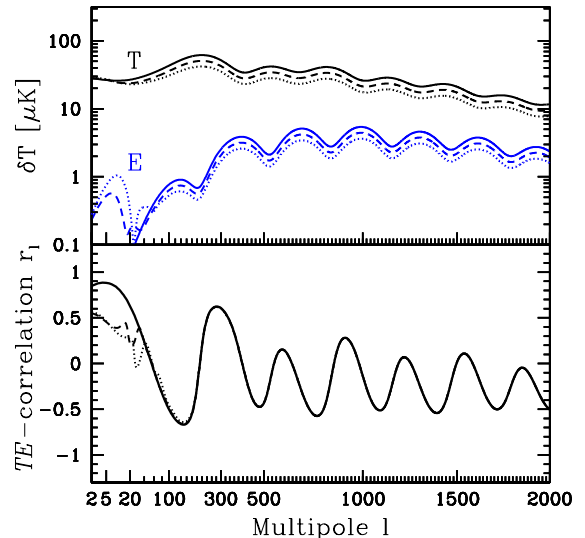


FIG. 2. Examples of CMB polarization, showing how the reionization optical depth τ affects the T and E power spectra (top) and the TE correlation r_ℓ (bottom). Solid, dashed and dotted curves correspond to $\tau=0, 0.2$ and 0.4 , respectively. As discussed in [23], changing the cosmological parameters affects the polarized and unpolarized power spectra rather similarly except for the cases of reionization and gravitational waves. In the reionization case, a new series of peaks are generated at large scales. *Top-panel:* Although there is no visible change in T at large scales, there is clearly a visible change in E since the Sachs-Wolfe nuisance is unpolarized and absent. *Lower-panel:* On small scales, reionization leaves the correlation r_ℓ unchanged since C_ℓ^T and C_ℓ^E are merely rescaled. On very large scales, r_ℓ drops since the new polarized signal is uncorrelated with the old unpolarized Sachs-Wolfe signal. On intermediate scales $\ell \gtrsim 20$, oscillatory correlation behavior is revealed for the new peaks. For more details about CMB polarization and reionization see [43]

II. PHENOMENOLOGY

A. Notation

CMB measurements can be decomposed into three maps (T, E, B), where T denotes the unpolarized and (E, B) denotes the polarized components, respectively. From these three maps we can measure a total of six angular power spectra, here denoted by $C_\ell^T, C_\ell^E, C_\ell^B, C_\ell^X, C_\ell^Y$ and C_ℓ^Z , corresponding to the TT, EE, BB, TE, TB and EB correlations*, respectively.

* From here on, we adopt the notation $TT \equiv T, EE \equiv E, BB \equiv B, TE \equiv X, TB \equiv Y$ and $EB \equiv Z$.

By parity, $C_\ell^Y = C_\ell^Z = 0$ for scalar CMB fluctuations, but it is nonetheless worthwhile to measure these power spectra as probes of both exotic physics [44–46] and foreground contamination. $C_\ell^B = 0$ for scalar CMB fluctuations to first order in perturbation theory [30–33] – secondary effects such as gravitational lensing can create B polarization even if there are only density perturbations present [47]. Finally, in the absence of reionization, C_ℓ^E is typically a couple of orders of magnitude below C_ℓ^T on small scales and approaches zero on the very largest scales.

The cross-power spectrum C_ℓ^X is not well suited for the usual logarithmic power spectrum plot, since it is negative for about half of all ℓ -values [23]. A more convenient quantity is the dimensionless correlation coefficient

$$r_\ell^X \equiv \frac{C_\ell^X}{(C_\ell^T C_\ell^E)^{1/2}}, \quad (1)$$

plotted on a linear scale in Figure 2 (lower panel), since the Schwarz inequality restricts it to lie in the range $-1 \leq r_\ell^X \leq 1$. From here on we use r_ℓ as shorthand for r_ℓ^X . For more details about r_ℓ and how it depends on cosmological parameters, see section II.b in [23].

B. Our Knowledge of Synchrotron Emission

The Galactic InterStellar Medium (ISM) is a highly complex medium with many different constituents interacting through a multitude of physical processes. Free electrons spiraling around the Galactic magnetic field lines emit synchrotron radiation [48], which can be up to 70% linearly polarized (see [49,50] for a review).

The power spectrum \mathbf{C}_l of synchrotron radiation is normally modeled as a power law in both multipole ℓ and frequency ν , which we will parametrize as

$$\delta T_\ell^2(\nu) = A \left(\frac{\ell}{50} \right)^{\beta+2} \quad \text{with} \quad A \propto \nu^{-2\alpha}, \quad (2)$$

where $\delta T_\ell \equiv [\ell(\ell+1)C_\ell/2\pi]^{1/2}$. This definition implies that $\mathbf{C}_l \propto \ell^\beta$ for $\ell \gg 1$ and that the fluctuation amplitude $\propto \nu^{-\alpha}$. The standard assumption is that the unpolarized intensity has $\alpha \approx 2.8$ with variations of order 0.15 across the sky[†] [51].

[†] Because the spectral index α depends on the energy distribution of relativistic electrons [48], it may vary somewhat across the sky. One also expects a spectral steepening towards higher frequencies, corresponding to a softer electron spectrum ([52]; Fig 5.3 in [53]). A recent analysis done at 22 MHz [54] shows that α varies slightly over a large frequency range.

As to the power spectrum slope β , the 408 MHz Haslam map [55,56] suggests β of order 2.5 to 3.0 down to its resolution limit of $\sim 1^\circ$ [‡] [58–61]. A similar analysis done in the 2.3 GHz Rhodes map of resolution $20'$ [53] gives $\beta=2.92\pm0.07$ [62] (flattening to $\beta \approx 2.4$ at low Galactic latitudes [29]).

For the polarized synchrotron component, our observational knowledge is, unfortunately, not as complete. To date, there are measurements of the polarized synchrotron power spectrum obtained basically from three different surveys [63]: the Leiden surveys[§] [36,35], the Parkes 2.4 GHz Survey of the Southern Galactic Plane^{**} [39,40], and the Medium Galactic Latitude Survey^{††} [41,42,64]. These measurements exhibit a much bluer power spectrum in polarization than in intensity, with β in the range from 1.4 to 1.8 [4,24–29]. These results are usually taken with a grain of salt when it comes to their implications for CMB foreground contamination, for three reasons:

1. Extrapolations are done from low to high galactic latitudes;
2. Extrapolations are done from low to high frequencies; and
3. Much of the available data is undersampled.

The Leiden surveys extend to high Galactic latitudes and up to 1.4 GHz but are unfortunately undersampled, while the Parkes and the Medium Galactic Latitude Surveys only probe regions around the Galactic plane. In the following three sections, we will discuss these three problems in turn.

[‡] Although the interpretation is complicated by striping problems [57].

[§] The observations done by Brouw and Spoelstra covered almost 40% of the sky extending to high Galactic latitudes. Using the same instrument, they observed the polarized Galaxy in Q and U in five frequencies from 408 MHz up to 1.4 GHz and with angular resolutions from 2.3° at 408 MHz up to 0.6° at 1.4GHz. Unfortunately this data was also undersampled, making it difficult to draw inferences about its polarized power spectrum.

^{**} This survey covers a strip 127° long and at least 10° wide centered in the Galactic plane, with a resolution of FWHM= $10.4'$. It is publically available at <http://www.uq.edu.au/~roy/>.

^{††} The Medium Galactic Latitude Survey maps the Galactic plane within $\pm 20^\circ$, with a resolution of FWHM= $9.35'$ at 2.4 GHz. This survey is partially available at <http://www.mpifr-bonn.mpg.de/staff/buyaniker/index.htm>.

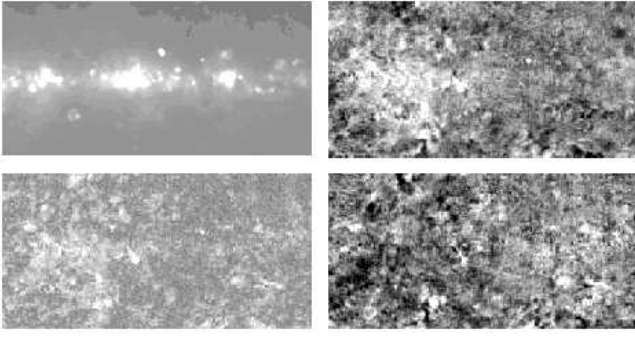


FIG. 3. The nature of the Galactic synchrotron emission. Clockwise from top left, the panels show Stokes T , U , Q , and P (defined as $P = \sqrt{Q^2 + U^2}$) from Block 3 of the Parkes 2.4 GHz Survey of the Southern Galactic Plane.

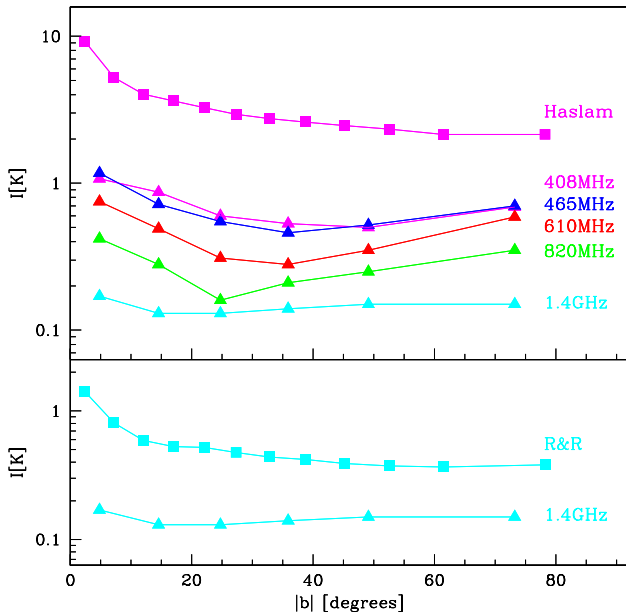


FIG. 4. The polarized and unpolarized synchrotron component as a function of the Galactic latitude. Each of five Leiden polarized surveys was divided in six slices of equal area, we then calculated the mean intensity (defined as $P = \sqrt{Q^2 + U^2}$) for each of those slices. A similar procedure was used for the unpolarized Haslam and Reich & Reich surveys, but 12 slices were chosen instead. The top panel show the results from the five Leiden surveys plus the 408 MHz Haslam data, while the bottom panel show the results from the Leiden 1.4 GHz survey and 1.42 GHz Reich & Reich data. Comparison between polarized and unpolarized components at the same frequency illustrates that the polarized synchrotron is almost independent of the Galactic latitude while the unpolarized emission is strongly concentrated in the Galactic plane.

1. The Latitude Extrapolation Problem

Although only high Galactic latitudes are relevant for CMB work, most of the data used for understanding the polarized CMB foreground contamination is at low Galactic latitudes. Figure 3 shows that whereas the unpolarized synchrotron emission depends strongly on the Galactic latitude, the polarized component is approximately independent of Galactic latitude — indeed, in the three polarized images, it is difficult to distinguish the galactic plane at all. As noticed a long ago by [40], there is a faint, quasi-uniform polarized component of the Galactic polarized emission in their survey, upon which the emission from other features is superimposed: towards the higher latitudes, this faint component appears similar in both structure and intensity to the correspondent lower latitude emission. This well-know empirical result can be also seen (in a more quantitative way) in the Leiden surveys. Figure 4 shows that in the frequency range between 408 MHz to 1.4 GHz, the Polarization Intensity P ($P = \sqrt{Q^2 + U^2}$) is basically constant as the Galactic latitude $|b|$ increases, whereas the unpolarized surveys (such as the 408 MHz Haslam and the 1420 MHz Reich & Reich [65]) have the bulk of their emission coming from the Galactic plane.

The usual interpretation for this very weak latitude dependence of polarized synchrotron radiation is that the signal is dominated by sources that are nearby compared to the scale height of the Galactic disk, with more distant sources being washed out by Depolarization (to which we return in the next subsection). As a result, having well-sampled polarized maps off the galactic plane at the same frequencies would not be expected to affect our results much, since they would be similar to those in the plane. This issue, however, deserves more work as far as extrapolation to CMB frequencies is concerned: the latitude dependence may well return at higher frequencies as Depolarization becomes less important, thereby revealing structure from more distant parts of the Galactic plane. In this case, extrapolating from an observing region around the Galactic plane to higher latitudes may well result in less small-scale power in the angular distribution.

If we are *lucky*, many of the complications of extrapolating to higher latitude may largely cancel out the complications of extrapolating to higher frequency, thereby making it easier to quantify the polarized CMB foreground problem. The reason for optimism is the following: At high latitudes (which is all that really matters for CMB research), the foreground signal will be entirely due to nearby emission within the scale height of the thick Galactic disk, and at low frequencies in the Galactic plane (which is where we have really good data), the polarized signal we see may well be dominated by such nearby emission, with emission from more distant regions in the Galactic disk hidden by Faraday Depolarization.

2. Faraday Rotation, Depolarization and the Frequency Extrapolation Problem

The plane of a polarized wave may be regarded as the sum of two circularly polarized components of opposite handedness. In an ionized medium with a non-zero magnetic field, these two components propagate with different phase velocities, which will result in a rotation of the plane of polarization of the linearly polarized radiation. This rotation, known as the Faraday Rotation[†], produces a change in polarization angle $\Delta\theta$ of

$$\Delta\theta = 0.81\lambda^2 \int_0^L n_e B_{\parallel} dL = \lambda^2 RM \text{ [rad]}, \quad (3)$$

where λ is the wavelength given in meters and the quantity $\Delta\theta/\lambda^2$ is called the Rotation Measure (RM – usually expressed in units of rad m^{-2}). The integral is done over the line of sight from us to the emitting region at a distance L in pc. n_e is the free electron density in cm^{-3} and B_{\parallel} is the magnetic field parallel to the line of sight in μG .

From equation (3) it is easy to see that observations of this synchrotron radiation in several frequencies allows the determination of Rotation Measures in the diffuse radiation. From the obtained structure in the Rotation Measure on different scales we can obtain information on the magnetic field parallel to the line of sight, weighted with electron density – an example of this method can be found in [68]. In radio astronomy, Faraday Rotation has become one of the main tools to investigate the interstellar magnetic field (see, *e.g.* [69,70]).

It is important to point out, however, that Faraday Rotation can only change the polarization angle and not the polarized intensity P . The fact that we do see structure in P that is not correlated with their counterpart in intensity T implies that part of the radiation has been depolarized [38]. A simple visual comparison of the unpolarized and polarized maps of the same region in the sky of the Parkes 2.4 GHz survey shows Depolarization at work (see Figure 3): many sources which present an intense unpolarized emission do not show a counterpart in the polarized maps; similarly bright regions of extended polarization are not connected with unpolarized sources. A more detailed study of this same survey reached similar conclusions: Giardino *et al.* [29] showed that the E and B power spectra were dominated by changes in the polarization angle rather than by changes in the polarized intensity, suggesting that Faraday Rotation was playing a significant role[‡].

Depending on the frequency and beamwidth used, Depolarization can play an important role in polarization studies of the Galactic radio emission [35]. As discussed by Cortiglioni and Spoelstra [71], Depolarization can have four causes: 1) differential polarization along the line of sight, 2) differential polarization across the beam, 3) differential Faraday Rotation across the beam, and 4) differential Faraday Rotation and polarization across the bandwidth. If the bandwidth is very narrow, we can neglect item 4; also, if the polarized data has been sufficiently sampled, smoothing it to a largest beam may inform us about items 2 and 3, leaving us with item 1 as the expected main source of Depolarization[§].

Because of the complicated interplay of these mechanisms, we should expect both the amplitude and the shape of the polarized synchrotron power spectrum to change with frequency. We will therefore take an empirical approach below and use the available data to map out (for the first time) the two-dimensional region in the (ℓ, ν) plane where Faraday Rotation and Depolarization are important.

that the polarized and unpolarized components are uncorrelated, [40] found that for some patches in their images there is a good correlation between the polarized and total power intensities. Therefore they conclude that a good fraction of the polarized emission seen over the plane was caused by changes in synchrotron emissivity, rather than any Depolarization or Faraday Rotation of the synchrotron background. According to [40], variations in synchrotron emission can be caused by increases in the density of relativistic electrons (due to SNRs), and/or variations in the magnetic field intensity.

It is important to point out that the relative importance of these two mechanisms (Faraday Rotation & Depolarization and changes in the synchrotron emissivity of the source regions) over the Galactic plane region are currently unknown [66].

[§] In the case of Leiden surveys, item 4 is negligible. Based in previous analysis done over the Galactic loops at 1.4 GHz [72,73], Spoelstra [35] argued that items 2 and 3 have a relatively minor contribution to the Depolarization in those surveys. Leaving, therefore, differential polarization along the line of sight as the main source of Depolarization.

[†] A detailed discussion of the Faraday Rotation and Depolarization effects as well as their importance in astrophysical observations is given in [67].

[‡] Although at first glance the images in Figure 3 suggest

For the case of undersampling in the Leiden surveys, some authors have overcome this problem by doing their Fourier analysis over selected patches in the sky where they believe the average grid space in the patch is close to the map’s beam size, so that they can apply a Gaussian smoothing on it – this is well explained and illustrated in [27]. Fortunately, we can eliminate this problem by measuring the power spectra with the matrix-based quadratic estimator technique that has recently been developed for analyzing CMB maps [74,75,23].

Although the undersampling and partial sky coverage results in unavoidable mixing between different angular scales ℓ and polarization types (E and B), this mixing (a.k.a. *leakage*) is fully quantified by the window functions that our method computes [75] and can therefore be included in the statistical analysis without approximations. Specifically, we compute the six power spectra (T, E, B, X, Y, Z) described in Section II A so that the leakage, if any, is minimal.

In [75] it was argued that susceptibility to systematic errors could be reduced by choosing the “priors” that determine the quadratic estimator method to have vanishing cross-polarizations, $X = Y = Z = 0$, and it was shown that this simplification came at the price of a very small (percent level) increase in error bars. In Appendix A of [23], it was shown that this choice has an important added benefit: exploiting a parity symmetry, it eliminates 14 out of the 15 leakages, with only the much discussed [75,32,76–79] $E - B$ leakage remaining. In [80] it was shown that even the remaining $E - B$ leakage can, in principle, be removed. Unfortunately, this technique cannot be applied here, since it works only for a fully sampled two-dimensional map.

III. RESULTS

A. POLAR Power Spectra

POLAR was a ground-based CMB polarization experiment that operated near Madison, Wisconsin [22,81,82]. It used a simple drift-scan strategy, with a 7° FWHM beam at 26–30 GHz, and simultaneously observed the Stokes parameters Q and U in a ring of declination $\delta = 43^\circ$. Because POLAR was insensitive to the unpolarized CMB component, we cross-correlate their Q and U data with the T -data from the *COBE*/DMR map [83].

We compute the six power spectra described in Section II A using the quadratic estimator method exactly as described in [75]. We computed fiducial power spectra with the CMBFAST software [84] using cosmological parameters from the concordance model from [85] (that of [86] is very similar). Table 1 shows the result of our band-power estimation. The values shown in parentheses in the rightmost column of this table are our $2\text{-}\sigma$ upper limits. In these calculations, we used 5 multipole bands of width $\Delta\ell = 6$ for each of the six polarization types (T, E, B, X, Y, Z), thereby going out to $\ell = 30$, and average the measurements together with inverse-variance weighting into a single number for each polarization type to minimize noise.

We used the combined DMR 53+90 GHz data to obtain good sensitivity to the unpolarized component. We perform our analysis using strips of the DMR data of width $\pm 15^\circ$ around the POLAR declination – we found that further increasing in the width of these disks did not significantly tighten our constraints. Finally, we eliminated sensitivity to offsets by projecting out the mean (monopole) from the T, Q and U maps separately.

The detection of unpolarized power is seen to be consistent with that published by the DMR [83] group. Table 1 shows that we detect no polarization or cross-polarization of any type, obtaining mere upper limits, just as the models predict. The window functions reveal substantial leakage between E and B , so that the limits effectively constrain the average of these two spectra rather than both separately. This large leakage is due to the one-dimensional nature of the POLAR dataset, and can be completely eliminated with a fully sampled two-dimensional map [80].

Finally, we perform the same analysis described above by replacing the DMR stripe with a similar stripe selected from the 408 MHz Haslam map (which was smoothed to 7° and scaled to 30 GHz using $\beta_T = -3$). We detected no cross-polarization of any type between POLAR and the Haslam map, obtaining a mere upper limit of $X \lesssim 8.6\mu K$ (or a $2\text{-}\sigma$ upper limit of $11.7\mu K$).

Table 1 – POLAR-DMR Power Spectrum

	$\ell_{\text{eff}} \pm \Delta\ell$	$\delta T^2 \pm \sigma [\mu K^2]$	$\delta T [\mu K]^{(a)}$
T	15.6 ± 6.6	487.0 ± 270.6	$22.1^{+7.4}_{-5.5}$
E	12.6 ± 4.5	-19.7 ± 63.9	$< 6.6(10.4)$
B	12.6 ± 4.5	27.7 ± 63.9	$< 9.6(12.5)$
X	14.0 ± 4.8	-36.7 ± 68.6	$< 5.6(10.0)$
Y	14.0 ± 4.8	-0.2 ± 68.6	$< 8.3(11.7)$
Z	11.4 ± 2.9	-100.0 ± 63.3	$< (5.2)$

^(a)Values in parentheses are $2\text{-}\sigma$ upper limits.

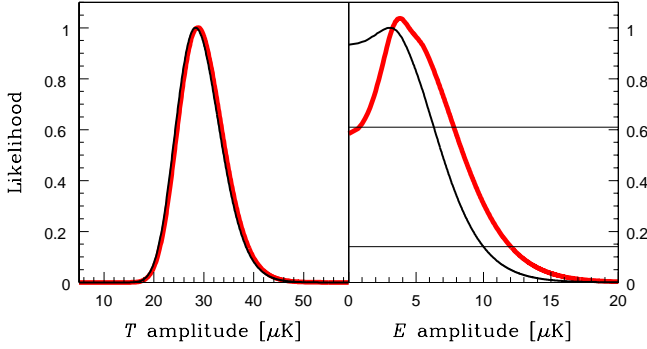


FIG. 5. Likelihood results using the E -polarized information alone (right panel, solid black line), using T information alone (left panel, solid black line), and using both POLAR and DMR T -information and marginalizing (solid red lines). From top to bottom, the two horizontal lines correspond to 68% and 95% confidence limits, respectively.

2. Likelihood Analysis

We complement our band-power analysis with a likelihood analysis where we assumed that $B = 0$. Specifically, we set $B = Y = Z = 0$ and take each of the remaining power spectra (T, E, X) to be constant out to $\ell = 30$.

We first perform a simple 1-dimensional likelihood analysis for the parameter E using the POLAR data alone (discarding the DMR information), obtaining the likelihood function in excellent agreement with that published by [22] – see Figure 5 (right panel, solid black line). A similar 1-dimensional likelihood analysis for the parameter T using the DMR data alone produces $T \approx 28 \mu\text{K}$, consistent with that of the DMR team [83] (left panel, solid black line). We then compute the likelihood function including both POLAR and DMR data in the 3-dimensional space spanned by (T, E, r_ℓ) and compute constraints on individual parameters or pairs by marginalizing as in [85]. Once again, we obtain a T -measurement in complete agreement with that for the DMR team (left panel, solid red line).

Figure 6 shows our constraints in the (E, r_ℓ) -plane after marginalizing over T . It is seen that our constraints on the cross-polarization are weaker than the Schwarz inequality $|r_\ell| \leq 1$, so in this sense the data has taught us nothing new. Since r_ℓ is expected to oscillate between positive and negative values, using a flat (constant) r_ℓ in the likelihood analysis runs the risk of failing to detect a signal that is actually present in the data, canceling out positive and negative detections at different angular scales. This is not likely to have been a problem in our case, since r_ℓ is uniformly positive in our sensitivity range $\ell = 14 \pm 5$ for the concordance model.

Figure 1 compares our results with all other polarization constraints published to date.

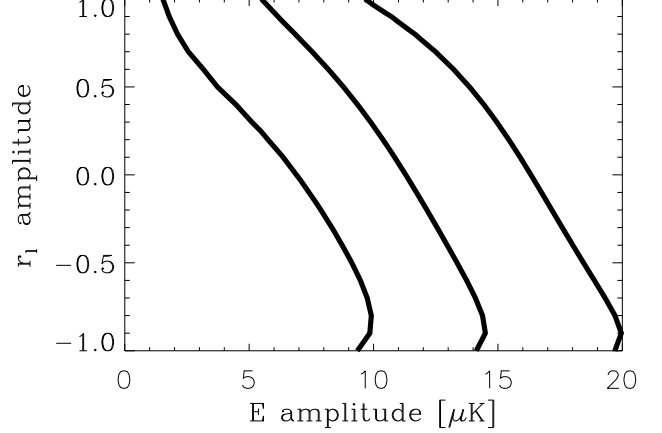


FIG. 6. Joint constraints on E polarization and r_ℓ after marginalizing over T . From left to right, the contours show that the likelihood function has dropped to $e^{-1.1}$, $e^{-3.0}$ and $e^{-4.6}$ times its maximum value, which would correspond to 68%, 95% and 99% limits if the likelihood were Gaussian. For comparison, the concordance model predicts $(E, r_\ell) = (0.001, 0.66)$ at $\ell = 14$, the center of our window function for X (see Table 1).

B. The Leiden Power Spectra

1. Basic power spectra

For the Leiden surveys, our analysis was performed using 10 multipole bands of width $\Delta\ell = 10$ for each of the six polarization types (T, E, B, X, Y, Z), thereby going out to $\ell = 100$. We used the Haslam map for the unpolarized component T , scaled and smoothed to match Leiden's five different frequencies. A Galactic cut of $|b| = 25^\circ$ was applied in order to match the POLAR observing region. We iterated the QE method once and chose the second prior to be a simple power law model consistent with the original measurement for the T , E and B power. The priors for X , Y and Z were set as zero.

Figure 7 shows the E power spectra (top) and r_ℓ correlation coefficient (bottom) of the Leiden surveys. We find that all power spectra are well approximated by power laws as in equation (2). The best fit normalizations A and slopes β for T , E and B are shown in Table 2. The values of β for E and B are consistent with previous analyses [4, 24–29], showing that the slopes get shallower as frequency increases.

For all Leiden surveys, X and Y power spectra are show to be consistent with zero – the 2.4 GHz Parkes survey had a similar finding for X [29]. These are not surprising results, but another indication that Depolarization is at work in these frequency ranges: assuming that Depolarization causes the polarized and unpolarized components to be uncorrelated (see Figure 3), it is

natural to expect that $X, Y=0$. However, at the CMB frequencies (where the effects of Faraday Rotation and Depolarization are unimportant) this should not be the case.

To study the frequency dependence, we average the 10 multipole bands of the Leiden power spectrum measurements together into a single band for each polarization type to reduce noise. From these results, we fit the average frequency dependence (for the 25° cut data) as a power law as in equation (2) with slope $\alpha_E = 1.3$ and $\alpha_B = 1.5$ for E - and B -polarization, respectively.

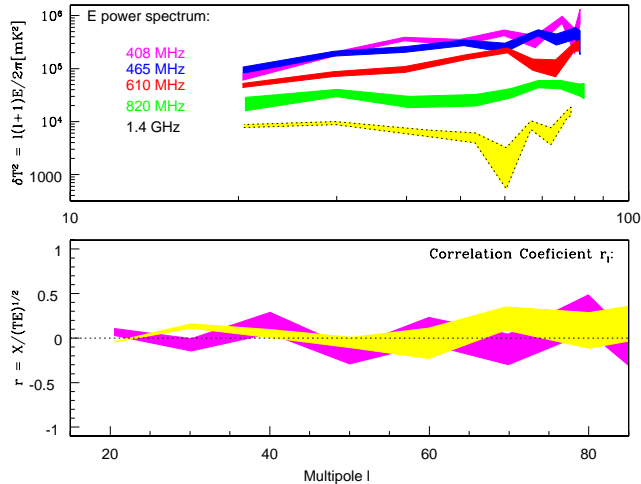


FIG. 7. Power spectra of the Leiden data. Top panel shows the E power spectra for the five Leiden frequencies going from 408 to 1411 MHz, while the Bottom panel shows the X cross power spectrum r_ℓ for two of the five Leiden frequencies (each frequency is represented by the same color in both plots). Intrinsic EB correlation could be present but masked by Faraday rotation, since random rotations of the polarization angle would cause correlations to average to zero.

Table 2 – Normalization & Spectral Index^(a)

ν (GHz)	A_E [mK ²]	β_E	A_B [mK ²]	β_B
0.408	5.5	-0.5	5.7	-0.4
0.465	5.4	-1.0	5.4	-0.5
0.610	5.1	-1.0	5.1	-0.8
0.820	4.5	-1.5	4.6	-1.8
1.411	3.9	-1.9	3.6	-2.6

^(a) All fits are normalized at $\ell=50$, i.e., $\delta T_\ell^2 = A(\ell/50)^{\beta+2}$.

2. Is it E or is it B ?

An interesting question about polarized foregrounds is how their fluctuations separate into E and B . Although many authors initially assumed that foregrounds would

naturally produce equal amounts of E and B , Zaldarriaga [77] shows that this should not be the case. There are plausible scenarios where the foreground polarization direction could preferentially be aligned with or perpendicular to the gradient of polarized intensity, thereby producing more E than B . In contrast, it is more difficult to contrive scenarios with more B than E , since they require polarizations preferentially making a 45° angle with the gradient.

Early studies [25,29] have indicated that $E \approx B$ at 2.4 GHz in the Galactic plane. These analyses however used Fourier transforms and spin-2 angular harmonic expansions, respectively, without explicitly computing the window functions quantifying the leakage between E and B . This leakage is expected to be important both on the scale of the Parkes stripe thickness and on the pixel scale [75,80], and would have the effect of mixing E and B power, reducing any E/B differences that may actually be present. Moreover, no study of the E/B ratio has ever been done on the large angular scales ($\ell \lesssim 40$) that are the most important for constraining reionization and inflationary gravity waves.

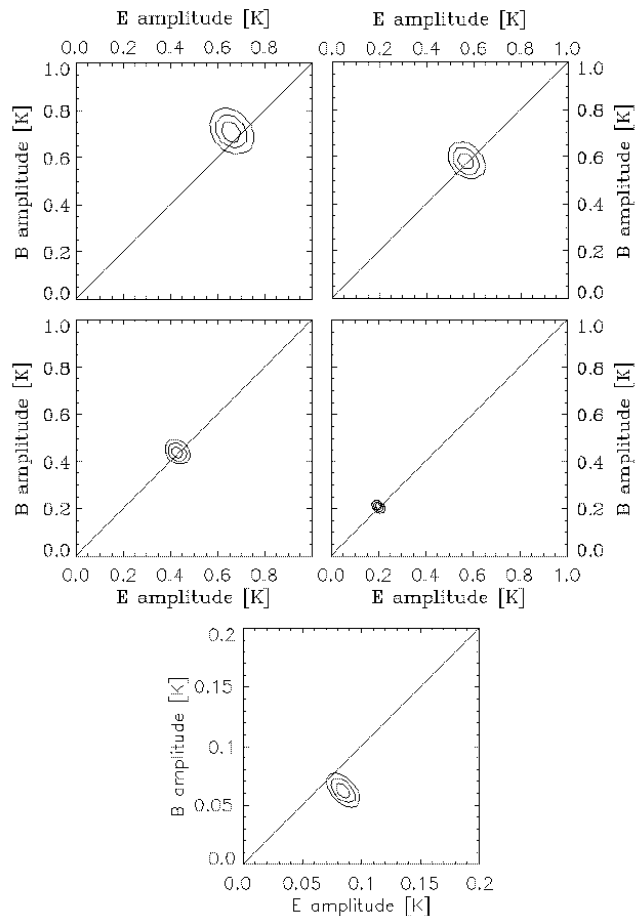


FIG. 8. E and B likelihood values for the Leiden surveys. From top to bottom, and from left to right, the likelihoods are for the frequencies 408, 465, 610, 820 and 1411 MHz. As the survey's frequency increases, the Faraday Rotation reduces and we start to see a slight hint of an E -excess. For all likelihoods, the contours correspond to 68%, 95% and 99% limits. The diagonal lines correspond to $E = B$.

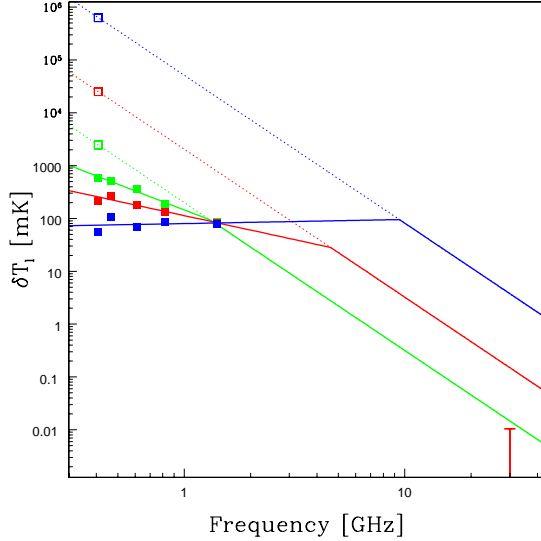


FIG. 9. The E -polarized (solid) and unpolarized (dashed) power spectra δT_ℓ of Galactic synchrotron emission are plotted as a function of frequency for multipoles $\ell = 2$ (blue), $\ell = 14$ (red) and $\ell = 50$ (green) using the fits from Table 2 (corresponding to a 25° Galactic cut data). The T curves (dashed) assume $\alpha = -2.8$. For comparison, the POLAR upper limit $E < 10.4 \mu\text{K}$ for $\ell \sim 14$ from Table 1 is shown in the lower right corner. Comparing this with the red curve implies either a low synchrotron polarization fraction or a steeper spectral index (lower α).

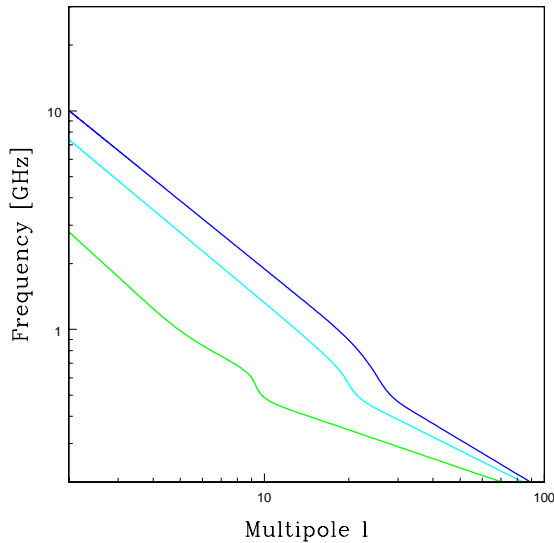


FIG. 10. (ℓ, ν) plane showing contours of constant Depolarization. From bottom to up the curves are for the 100%, 70% and 0% Depolarization percentage.

We therefore perform a likelihood analysis of the Leiden surveys specifically focusing on this question, and including an exact treatment of the leakage. The likelihood analysis of the data is done with two free parameters corresponding to the overall normalization of the E and B power spectra, and assuming that they both have the same power law shape given by the slopes β_E from Table 2. The results are shown in Figure 8. Note that the E and B amplitudes are consistent with being equal to high accuracy at 408, 465, 610 and 820 MHz. At the highest frequency of 1.4 GHz, however, we see a hint of an E -excess at the 30% level, but this is only significant at a level of around 95%. This hint is intriguing, since it can in principle be given a natural physical interpretation. It may be that synchrotron polarization has $E > B$ at CMB frequencies, and that Faraday rotation is hiding this underlying asymmetry at low frequencies. If the Faraday effect rotates each polarization angle by a for all practical purposes random amount, this will destroy any intrinsic alignment between the direction of the polarization and the direction of the local intensity gradient and therefore produce equal amounts of E and B signal.

3. Quantifying the Importance of Faraday Rotation & Depolarization for the CMB

The key challenge for modeling synchrotron polarization as a CMB foreground is to answer the following question: above which frequency are the effects of Faraday Rotation and Depolarization so small that our measurements can be safely extrapolated up to CMB frequencies? From an analysis of the Leiden surveys, Spoelstra [35] found an upper limit for RM of 35 rad m^{-2} . Setting $\Delta\theta = 1 \text{ rad}$ in equation (3), this suggests that the Faraday Rotation becomes irrelevant somewhere around 2 GHz. However, considering that the determination of RM is poor in many parts of these surveys, this 2 GHz value is questionable. Moreover, because of the importance of Depolarization which affects small scales more than large scales, we should expect the answer to depend on the angular scale ℓ considered.

Let us now quantify this empirically. Figure 9 shows the synchrotron power spectra as a function of frequency for a sample of angular scales ℓ . Using the fits from Table 2 and Equation (2) suggests that the polarization percentage $p \equiv \delta T_\ell^E / \delta T_\ell^T$ saturates to a constant value for $\nu \gg 1 \text{ GHz}$ at $\ell=50$, $\nu \gg 4 \text{ GHz}$ at $\ell=14$ and $\nu \gg 10 \text{ GHz}$ at $\ell=2$. This suggest the following universal behavior. At high frequencies, where the Faraday Rotation & Depolarization effects are unimportant and the polarized fluctuations simply constitute some constant fraction of the unpolarized fluctuations, we can use the

same α for polarized and unpolarized synchrotron radiation in the CMB range. However, moving to the left in Figure 9, one reaches a critical frequency ν_* below which the Faraday effects suppress the polarized fluctuations. At this point, the power law changes asymptotes from a steeper (solid lines) to a shallower (dashed lines) power law, and the critical frequency ν_* in which this effect occurs change with the angular scale ℓ . In other words, whether we can safely extrapolate our results up to CMB frequencies depends not only on the frequency but also in the angular scale. For instance, the contamination of the CMB quadrupole from Galactic synchrotron polarization can only be obtained from extrapolations of data at frequencies exceeding $\nu_* \sim 10$ GHz, with ν_* dropping towards smaller angular scales.

All the information above is summarized in Figure 10, which shows contours of constant polarization fraction $p = \delta T_\ell^E / \delta T_\ell^T$ in the two-dimensional (ℓ, ν) plane. In other words, this figure can be interpreted as a contour plot of the depolarization. The depolarization is seen to be negligible at high frequencies and on tiny scales, gradually increasing towards the lower left corner (towards low frequencies and on large angular scales) where Faraday effects become important.

This has important implications. For instance, a nice all-sky simulation of synchrotron polarization at CMB frequencies was recently performed assuming that the power spectra of $\cos 2\phi$ and $\sin 2\phi$ were frequency independent [29], where ϕ is the polarization angle. Our results indicate that these two power spectra are dominated by Faraday effects, which implies that the E and B power should be mostly due to changes in polarization angle, not to variations in overall intensity — precisely this behavior is indeed seen by [29]. If Faraday effects are indeed dominant, then it is not obvious that such frequency extrapolation of the $\cos 2\phi$ and $\sin 2\phi$ power spectra are valid.

t Figure 9 also shows the POLAR limit $E < 10.4\mu K$ from Table 1, in the lower right corner. Since this limit corresponds to $\ell \sim 14$, it can be directly compared with the middle (red) curve. The noticeable gap between the two implies that we get interesting constraints on foreground models. No synchrotron polarization is detected even though the Haslam map shows substantial synchrotron emission in the POLAR region, so either the synchrotron polarization fraction is small or the synchrotron emission falls even more steeply towards higher frequencies than the plotted curves indicate. A spectral index $\alpha = -2.8$ as in the plot is only allowed if the polarization fraction $p < 10\%$. If $p = 20\%$, then $\alpha < -3.0$, and almost complete polarization (about 70% is physically possible) would require $\alpha < -3.4$, in poor agreement with theoretical and observational indications [52–54]. In other words, our results suggest a rather low synchrotron polarization fraction at CMB frequencies.

IV. CONCLUSIONS

CMB polarization and its decomposition into E and B modes is a topic of growing importance and interest in cosmology. In the era of MAP, a key issue is to estimate the contribution of Galactic foregrounds (more specifically, polarized synchrotron emission) to these modes. We have used the POLAR experiment and radio surveys in order to quantify this contribution at large angular scales.

Using matrix-based quadratic estimator methods, we cross-correlated POLAR with DMR data and obtained upper limits $E < 10.4\mu K$ and $|X| < 10.0\mu K$ at 95% confidence. These upper limits are, unfortunately, too high to place interesting constraints on reionization models. A similar cross-correlation analysis was performed by replacing the DMR with the Haslam data, obtaining an upper limit $|X| \lesssim 11.7\mu K$ at 95% confidence.

We also used our quadratic estimator methods to measure the power spectra from the Leiden surveys, obtaining the following key results:

1. The synchrotron E - and B -contributions are equal to within 10% from 408 to 820 MHz, with a hint of E -domination at higher frequencies. One interpretation is that $E > B$ at CMB frequencies but that Faraday rotation mixes the two at low frequencies.
2. Faraday Rotation and Depolarization effects depend not only on frequency but also on angular scale — they are important at low frequencies ($\nu \lesssim 10$ GHz) and on large angular scales.
3. To extrapolate radio survey results from low to high galactic latitudes and from low to high frequencies, these Faraday effects must be taken into account.
4. We detect no significant synchrotron TE cross correlation coefficient ($|r| \lesssim 0.2$), but Faraday rotation could have hidden a substantial correlation detectable at CMB frequencies.
5. Combining the POLAR and radio frequency results, the fact that the E -polarization of the abundant Haslam signal in the POLAR region is not detected at 30 GHz suggests that the synchrotron polarization fraction at CMB frequencies is rather low.

Experiments such as MAP and Planck will shed significant new light on synchrotron polarization and allow better quantification of its impact both on these experiments and on ground-based CMB observations.

This work was supported by NSF grants AST-0071213 & AST-0134999, NASA grants NAG5-9194 & NAG5-11099. MT acknowledges a David and Lucile Packard Foundation fellowship and a Cottrell Scholarship from Research Corporation.

-
- [1] J. Kovac *et al.*, astro-ph/0209478 (2002).
- [2] M. Zaldarriaga, D. N. Spergel, and U. Seljak, ApJ **488**, 1 (1997).
- [3] D. J. Eisenstein, W. Hu, and M. Tegmark, astro-ph/9807130 (1998).
- [4] M. Tegmark, D. J. Eisenstein, W. Hu, and A. de Oliveira-Costa, ApJ **530**, 133 (2000).
- [5] M. Kaplinghat *et al.*, astro-ph/0207591 (2002).
- [6] A. A. Penzias and R. W. Wilson, ApJ **142**, 419 (1965).
- [7] N. Caderni, Phys.Rev. D **17**, 1908 (1978).
- [8] G. Nanos, ApJ **232**, 341 (1979).
- [9] P. M. Lubin and G. F. Smoot, Phys.Rev. Lett. **42(2)**, 129 (1979).
- [10] P. M. Lubin and G. F. Smoot, ApJ **245**, 1 (1981).
- [11] G. Sironi, G. Boella, G. Bonelli, L. Brunetti, F. Cavaliere, M. Fervasi, G. Giardino, and A. Passerini, New Astronomy **3**, 1 (1998).
- [12] P. M. Lubin, P. Melese, and G. F. Smoot, ApJ **273**, 51 (1983).
- [13] E. J. Wollack, N. C. Jarosik, C. B. Netterfield, L. A. Page, and D. Wilkinson, ApJ **419**, 49 (1993).
- [14] C. B. Netterfield *et al.*, ApJ **474**, 47 (1997).
- [15] E. Torbet, M. J. Devlin, W. B. Dorwart, T. Herbig, A. D. Miller, M. R. Nolte, L. A. Page, J. Puchalla, and H. Tran T, ApJ **521**, 79 (1999).
- [16] R. B. Partridge, J. Nawakowski, and H. M. Martin, Nature **311**, 146 (1988).
- [17] E. B. Fomalont, R. B. Partridge, J. D. Lowenthal, and R. A. Windhorst, ApJ **404**, 8 (1993).
- [18] R. B. Partridge, E. A. Richards, E. B. Fomalont, K. I. Kellerman, and R. A. Windhorst, ApJ **483**, 38 (1997).
- [19] R. Subrahmanyam, M. J. Kesteven, R. D. Ekers, M. Sinclair, and J. Silk, MNRAS **315**, 808 (2000).
- [20] G. F. Smoot, astro-ph/9902027 (1999).
- [21] M. Hedman *et al.*, astro-ph/0204438 (2002).
- [22] B. Keating *et al.*, ApJ **560**, 1 (2001).
- [23] A. de Oliveira-Costa, M. Tegmark, M. Zaldarriaga *et al.*, astro-ph/0204021 (2002).
- [24] M. Tucci, E. Carretti, S. Cecchini, R. Fabbri, M. Orsini, and E. Pierpaoli, astro-ph/0006387 (2000).
- [25] C. Baccigalupi, C. Burigana, Perrotta F, G. De Zotti, L. La Porta, D. Maino, M. Maris, and R. Paladini, astro-ph/0009135 (2000).
- [26] C. Burigana, and L. La Porta, astro-ph/0202439 (2002).
- [27] M. Bruscoli, M. Tucci, V. Natale, E. Carretti, R. Fabbri, C. Sbarra, and S. Cortiglioni, astro-ph/0202389 (2002).
- [28] M. Tucci, E. Carretti, S. Cecchini, L. Nicastro, R. Fabbri, B. M. Gaensler, J. M. Dickey, and N. M. McClure-Griffiths, astro-ph/0207237 (2002).
- [29] G. Giardino, A. J. Banday, K. M. Gorski, K. Bennett, J. L. Jonas, and J. Tauber, A&A;387:82 (2002).
- [30] A. Kamionkowski, A. Kosowsky, and A. Stebbins, Phys.Rev. D **55**, 7368 (1997).
- [31] M. Zaldarriaga and U. Seljak, Phys.Rev. D **55**, 1830 (1997).
- [32] M. Zaldarriaga, ApJ **503**, 1 (1998).
- [33] W. Hu, and M. White, Phys.Rev. D **56**, 596 (1997).
- [34] G. Westerhout, C. L. Seeger, W. N. Brouw, and Tinbergen J, Bull. Astron. Inst. Neth. **16**, 187 (1962).
- [35] T. A. T Spoelstra, A&A **135**, 238 (1984).
- [36] W. N. Brouw and T. A. T Spoelstra, A&AS **26**, 129 (1976).
- [37] N. Junkes, E. Fuerst, and Reich W, A&ASS **69**, 451 (1987).
- [38] M. H. Wieringa, A. G. De Bruyn, D. Jansen, W. N. Brouw, and P. Katgert, A&A **268**, 215 (1993).
- [39] A. R. Duncan, R. T. Stewart, R. F. Haynes, and K. L. Jones, MNRAS **277**, 36 (1995).
- [40] A. R. Duncan, R. F. Haynes, K. L. Jones, and R. T. Stewart, MNRAS **291**, 279 (1997).
- [41] B. Uyaniker, E. Fuerst, W. Reich, P. Reich, and R. Wielebinski, astro-ph/9807013 (1999).
- [42] B. Uyaniker, E. Fuerst, W. Reich, P. Reich, and R. Wielebinski, astro-ph/9905023 (1999).
- [43] M. Zaldarriaga, Phys.Rev. D **55**, 1822 (1997).
- [44] M. Kamionkowski, and A. Kosowsky, Ann.Rev. Nucl. Part. Sci. **49**, 77 (1999).
- [45] X. Chen, and M. Kamionkowski, Phys.Rev. D **60**, 104036 (1999).
- [46] M. Kamionkowski, and A. H. Jaffe, Int.J.Mod.Phys. A **16**, 116 (2001).
- [47] M. Zaldarriaga, and U. Seljak, Phys.Rev. D **580**, 3003 (1998).
- [48] G. B. Rybicki and A. P. Lightman, Radiative Processes in Astrophysics, p.167-194 (1979).
- [49] R. D. Davies and A. Wilkinson, astro-ph/9804208 (1998).
- [50] G. F. Smoot, in ASP Conf.Ser., Microwave Foregrounds, ed. A. de Oliveira-Costa & M Tegmark (San Francisco:ASP), 61(1999).
- [51] P. Platania *et al.*, ApJ **505**, 473 (1998).
- [52] A. J. Banday and A. W. Wolfendale, MNRAS **248**, 705 (1991).
- [53] J. L. Jonas, Ph.D. Thesis, Rhodes University (South Africa), p. (1999).
- [54] R. S. Roger, C. H. Costain, T. L. Landecker, and C. Swerdlyk M, astro-ph/9902213 (1999).
- [55] C. G. T Haslam *et al.*, A&A **100**, 209-219 (1981).
- [56] C. G. T Haslam *et al.*, A&AS **47**, 1 (1982).
- [57] D. Finkbeiner *et al.*, in preparation (2002).
- [58] M. Tegmark, and G. Efstathiou, MNRAS **281**, 1297 (1996).
- [59] F. R. Bouchet, R. Gispert, and J. L. Puget, in AIP Conf.Proc. 348, Unveiling the CIB, ed. E. Dwek (Baltimore:AIP), 225p. (1996).
- [60] F. R. Bouchet, and R. Gispert, NewA **4**, 443 (1999).
- [61] A. de Oliveira-Costa, M. Tegmark, D. Finkbeiner *et al.*, ApJ **530**, 133 (2002).
- [62] G. Giardino, A. J. Banday, P. Fosalba, K. M. Gorski, J. L. Jonas, W. O'Mullane, and J. Tauber, astro-ph/0103233 (2001).
- [63] W. Reich, E. Fuerst, P. Reich, R. Wielebinski, and M. Wolleben, astro-ph/0111437 (2001).
- [64] A. R. Duncan, P. Reich, W. Reich, and E. Fuerst, A&A **350**, 447 (1999).
- [65] P. Reich and W. Reich, A&ASS **74**, 7 (1998).
- [66] A. R. Duncan, in Galactic Foreground Polarization, ed. E.M. Berkhuysen (Bonn), 58 (1999).
- [67] D. D. Sokoloff, A. A. Bykov, A. Shukurov *et al.*, MNRAS **299**, 189 (1998).

- [68] K. Rohlfs, and T. L. Wilson, Tools of Radio Astronomy, p. 43-47 (1996)
- [69] M. Haverkorn, P. Katgert, and A. G. de Bruyn, (2000). astro-ph/0003260
- [70] B. M. Gaensler, J. M. Dickey, N. M. McClure-Griffiths, N. S. Bizunok, and A. J. Green, astro-ph/0010518 (2001).
- [71] S. Cortiglioni and T. A. T Spoelstra, A&A **302**, 1 (1995).
- [72] T. A. T Spoelstra, A&A **13**, 237 (1971).
- [73] T. A. T Spoelstra, A&A **21**, 61 (1972).
- [74] J. R. Bond, A. H. Jaffe, and L. E. Knox, ApJ **533**, 19 (2000).
- [75] M. Tegmark and A. de Oliveira-Costa, Phys.Rev. D **64**, 063001 (2001).
- [76] A. H. Jaffe, M. Kamionkowski, and L. Wang, Phys.Rev. D **61**, 083501 (2000).
- [77] M. Zaldarriaga, astro-ph/0106174 (2001).
- [78] A. Lewis, A. Challinor, and N. Turok, Phys.Rev. D **65**, 023505 (2002).
- [79] E. F. Bunn, astro-ph/0108209 (2001).
- [80] E. F. Bunn, M. Zaldarriaga, M. Tegmark, and A. de Oliveira-Costa, astro-ph/0207338 (2002).
- [81] B. Keating *et al.*, astro-ph/0111276 (2002).
- [82] C. O'Dell *et al.*, in preparation (2002).
- [83] G. F. Smoot *et al.*, ApJ **396**, 1 (1992).
- [84] U. Seljak, and M. Zaldarriaga, ApJ **469**, 437 (1996).
- [85] X. Wang, M. Tegmark, and M. Zaldarriaga, astro-ph/0105091 (2001).
- [86] G. Efstathiou *et al.*, astro-ph/0109152 (2001).